RevMexAA (Serie de Conferencias), **3**, 181–188 (1995)

X-RAYS FROM MASS LOADED SUPERNOVA REMNANTS

S. J. Arthur and W. J. Henney
Instituto de Astronomía, UNAM, Apdo. Postal 70-264, 04510 México D. F., México

RESUMEN

Observaciones de rayos-X provenientes de regiones H II alrededor de asociaciones de estrellas OB en la Nube Mayor de Magallanes han revelado luminosidades de rayos-X que no se pueden explicar por vientos estelares ni por remanentes de supernovas evolucionando dentro de las burbujas formadas por los vientos estelares. En este trabajo se propone un modelo en donde un remanente de supernova evoluciona dentro de una burbuja de densidad extremadamente baja (formada por la asociación de estrellas OB), pero la densidad en el remanente está realzada por la masa proveniente de condensaciones densas y frías que están inmersas en el flujo detrás de la onda de choque. Se encuentra que tales remanentes cargados de masa pueden explicar de una manera natural muchas de las propiedades enigmáticas de la emisión difusa de rayos-X observada.

ABSTRACT

Analysis of X-ray observations of H II complexes surrounding OB associations in the Large Magellanic Cloud have revealed X-ray luminosities that cannot be explained by stellar winds alone, nor by supernova remnants (SNR) evolving inside stellar wind bubbles. In this paper we propose a model in which a SNR evolves inside an extremely low density stellar wind bubble (formed by the OB association stars), but the density in the SNR is augmented due to hydrodynamic ablation of cool, dense clumps by the post blast wave SNR flow. Such mass loaded SNRs are found to explain in a natural way many of the puzzling properties of the observed diffuse X-ray emission.

Key words: **HYDRODYNAMICS — ISM: BUBBLES — ISM: SUPERNOVA REMNANTS — STARS: MASS LOSS — X-RAYS: INTERSTELLAR**

1. INTRODUCTION

Recent studies of the diffuse X-ray emission associated with clusters of OB stars in the Large Magellanic Cloud (LMC) (Chu & Mac Low 1990, hereafter CML90; Wang & Helfand 1991, hereafter WH91) have revealed X-ray luminosities far higher than can be explained by stellar winds alone, or by classical supernova remnants evolving inside these bubbles. In neither case would there be enough matter inside the bubbles to produce the observed flux. The diffuse emission has luminosities in the range 2×10^{34} (the detection threshold) to 10^{36} erg s^{-1}. These luminosities require temperatures of $T \sim 10^6$ K and densities of $n \sim 0.1$ cm^{-3} throughout the X-ray emitting region. Although a shocked stellar wind can easily have a temperature in excess of 5×10^6 K, the number density in the shocked wind region of a bubble of radius 50 pc (a typical radius for the bubbles surrounding OB associations in the LMC) will be of order 10^{-3} cm^{-3}. Obviously, for this reason, the observed emission cannot come from such a simple stellar wind bubble. The additional mass contribution from a supernova exploding inside such a stellar wind bubble would not be more than a few solar masses and so a supernova remnant evolving inside a stellar wind bubble could not add more than some 5×10^{33} erg s^{-1} to the total luminosity. An alternative explanation for the excess diffuse X-ray emission is therefore required.

CML90 proposed a model in which a supernova explodes off-center in a stellar wind bubble. However, their calculations just track the shock front of an adiabatic blast. Arthur & Falle (1991, 1993) show that

the flow *inside* a supernova remnant resulting from an explosion at (or near) a density interface is extremely complicated and mass from the denser part of the remnant is transported, due to large pressure gradients, to the less dense parts of the remnant, cooling adiabatically as it goes. It is therefore extremely unlikely that the model proposed by CML90 would result in an increase in the X-ray luminosity for any appreciable amount of time. WH91 proposed that the X-ray emission should last for some 10^5 yr to be consistent with star-formation and supernova rates in the LMC. An off-center supernova remnant is more likely to lead to short-lived X-ray flashes as the blast wave collides with the different parts of the bubble wall.

In this paper we propose a model in which mass from cool, dense clumps embedded in the stellar wind bubble mass loads the post blast-wave flow of a supernova remnant by a process of hydrodynamic ablation. The enhanced density and thermalization of the remnant produced by this mass loading process then give rise to the excess diffuse X-ray emission.

2. HYDRODYNAMIC ABLATION AND CLUMPS

It is unlikely that a stellar wind bubble will be completely homogeneous. Strong, slow stellar winds can be clumpy while Rayleigh-Taylor and Vishniac (Vishniac 1983) instabilities induced in the cold, dense shells of swept up ISM and previously ejected stellar material can cause them to fragment (García-Segura & Mac Low 1995). In addition, there will be clumps and inhomogeneities already existing in the ISM that are later overtaken by the wind bubble. Moreover, SNR such as Cassiopeia A show that some supernovae explode as "shrapnel bombs" with many pieces of ejecta thrown out into the surrounding medium. Such clumpy ejecta could be due to Rayleigh-Taylor instabilities during the explosion.

The lifetime of an individual clump once inside the remnant will depend on factors such as its size and density. It is assumed in this work that all the clumps are small, so that they would not cause the blast wave to deform to any great extent.

Hydrodynamic mass loading of astrophysical flows has been shown to have a significant effect on their dynamical evolution and cooling properties (Hartquist et al. 1986, hereafter HDPS; Arthur, Dyson, & Hartquist 1993, 1994, hereafter ADH1 and ADH2). The rate at which mass from a dense embedded clump enters the surrounding tenuous medium depends on the Mach number of this flow. For subsonic flows, the mass loading results from the lateral expansion of the clump due to pressure differences along its surface. In the supersonic case, mixing of the clump material into the surrounding flow will occur in the region of the turbulent wake behind the clump. It can be shown that the mass loading rate, $\dot{Q}$, in these two cases is given by

$$\dot{Q} = \begin{cases} QM^{4/3} & M < 1 \quad \text{(subsonic)} \\ Q \ \text{(constant)} & M \geq 1 \quad \text{(supersonic)} \end{cases} , \tag{1}$$

where M is the Mach number of the flow (HDPS) and Q is the maximum mass loading rate.

It has been found that mass loading tends to make supersonic flows subsonic and vice-versa, which, for a high enough mass loading rate, leads to a statistically transonic flow in which the pressure becomes important (HDPS; Dyson & Hartquist 1992). This was borne out by numerical calculations of stellar winds in Wolf-Rayet wind-blown bubbles and in planetary nebulae (ADH1; ADH2). As well as the effect on the dynamics, mass loading of an SNR will increase the amount of mass swept up by the remnant and hence affect its energetics and observational properties. Furthermore, the ionization structure inside a SNR evolving inside a clumpy bubble will not be in collisional equilibrium, since material ablated from the cool, dense clumps will generally be in a lower ionization state than the material of the hot, diffuse bubble and ionization timescales will be greater than dynamic timescales for such diffuse media.

Hydrodynamic ablation will dominate conductive evaporation for clumps embedded in hot, flowing plasmas since in this case conduction will be inhibited by the bending of magnetic field lines back around the clumps (Hartquist & Dyson 1993). For recent numerical results supporting this argument see Mac Low et al. (1994).

3. SNR EVOLUTION IN A STELLAR WIND BUBBLE

The standard picture of supernova remnant evolution does not obtain when this evolution occurs in a very diffuse medium. In order to progress from the initial free expansion stage (characterized by negligible pressure in the remnant and a linear velocity distribution) to the adiabatic stage (when the ejecta have been thermalized by the passage of a reverse shock) a remnant needs to have swept up more than 50 times the ejecta mass (Gull 1973). A Type II remnant (of initial ejecta mass greater than 5 $M_\odot$) evolving inside a diffuse stellar wind bubble

of typical density 10^{-3} cm^{-3} would have to have a radius of more than 135 pc before it entered the adiabatic phase. Few stellar wind bubbles are as large as this, and so the remnant will traverse the stellar wind bubble while still in free expansion then crash into the dense bubble wall. This interaction produces a transmitted shock propagating into the dense material surrounding the stellar wind bubble and a reflected shock propagating back into the bubble. The transmitted shock has a low velocity and will be radiative. The reflected shock propagates back through the bubble thermalizing the remnant as it goes. The X-ray emission produced by remnants in stellar wind bubbles (Type II) is therefore likely to be very different from that produced by remnants evolving in "standard" uniform media (Type Ia).

Mass loading of a supernova remnant evolving in a very diffuse medium can alter the above description of remnant evolution even further. Mass loading is most efficient in regions where the Mach number is unity or above. This means that while it is traversing the bubble in free expansion, the mass loading rate will be highest for those parts of the remnant where the pressure (and hence the temperature, or sound speed) is negligible. Adding mass to this part of the remnant helps to thermalize it much earlier than waiting for a reverse shock to pass through it. Mass loading in the region of swept up bubble material is much less efficient but equally effective, since in this part of the remnant the amount of mass swept up is so small, because of the extremely low densities, that the mass loaded material can dominate.

4. NUMERICAL METHOD

4.1. Hydrodynamics

In this work, a Godunov-type scheme (Godunov 1959) is used to follow the hydrodynamic evolution of the supernova remnant as it crosses the stellar wind bubble. This is a robust method that copes well with the interaction of the supernova remnant with the abrupt density changes encountered in the models. Such a method solves the Riemann problem at the interface between each pair of adjacent cells, and calculates the hydrodynamic flux between the cells based on the resultant state of the physical variables (density, pressure and velocity) that come from the solution of these Riemann problems. The scheme used is actually a second order (in space and time), spherically-symmetric Eulerian Godunov-type method (Arthur 1991; Falle 1991) that resolves shocks over about 4 – 5 grid cells. An Eulerian method has to be used because of the mass loading, since the amount of mass that is added to each cell at any particular time-step depends on the Mach number of the flow there and hence will be different in each cell and at each time-step. For a fuller discussion of the numerical method see Arthur & Henney (1995).

It is assumed that the clumps are at rest in the frame of the star, and hence do not contribute momentum to the flow. Their contribution to the energy equation is due to their ionization state and, as such, comes into the cooling source term. The cooling that each gas element of the SNR undergoes is due to collisionally excited line radiation, Bremsstrahlung, radiative recombination and collisional ionization. In this work we assume that the kinetic temperature of the ions and electrons and the excitation temperature of the ions are all equal.

4.2. Ionization State

In order to be able to calculate the X-ray emission from the SNR the ionization state in each grid cell of the numerical calculation needs to be known. If it is assumed that collisional ionization equilibrium holds throughout the remnant, then the ionization state is simply a function of the temperature in each cell. However, to investigate the *non-equilibrium* effects of adding cool mass to a hot flow, the ionization state must be evolved together with the hydrodynamics, taking into account the collisional ionization and radiative recombination rates of each ion stage under consideration.

All ionization stages of 13 elements (the most abundant) are included in the calculations. A look-up table of collisional ionization and radiative recombination rates generated by the Raymond-Smith code (Raymond & Smith 1976) is used, since these just depend on the temperature at the low densities encountered in this problem. Charge transfer reactions of certain metals with H and He are also tabulated, since recombination due to these processes may become important if low-ionization state hydrogen from clumps is added to high-ionization state metals in the hot plasma.

To make the calculation of the ionization state more efficient, we have employed the concept of "meta-ions" (Hamilton, Sarazin, & Chevalier 1983). These are groups of adjacent ion stages, whose ionization and recombination timescales are so much faster than the cooling timescale for the gas parcel that they can be

considered to be in relative equilibrium. By calculating the evolution of these meta-ions instead of the individual ion stages, a vast saving in computational costs can be achieved (Arthur & Henney 1995).

In this work two sets of abundances are used: galactic SNR (Cygnus Loop) and abundances appropriate to H II regions in the LMC collected from several sources (Dufour 1984; Russell & Dopita 1990, 1992; Pagel 1993). Where the Cygnus Loop abundance data are missing, solar abundances are adopted (Anders & Grevesse 1989). The different abundances will lead to differences in the cooling and in the resultant X-ray spectrum.

5. MODELS

5.1. Initial Conditions

We wish to investigate the effect of different mass loading rates on the evolution of supernova remnants inside diffuse stellar wind bubbles. In order to facilitate comparison between the different models, most of the parameters are kept constant and only the mass loading rate is changed. For one of the models different abundances are used. A bubble radius of 50 pc is adopted as being the most interesting for investigation since there exist X-ray observations of the bubble N51D in the LMC (which has a radius of about 53 pc) with which quantitative comparisons can be made.

The supernova ejecta have a modest (gas) mass of 5 $M_\odot$ and the energy of the explosion is 0.8×10^{51} erg. The ejecta are allowed to expand freely, according to the Gull (1973) model, up to a (piston) radius of 0.05 pc, at which point they begin to interact with a dense circumstellar medium. This circumstellar medium is assumed to have been formed during a dense, slow stellar wind phase, and so has a density profile that falls as $1/r^2$ and extends out to a radius of 0.15 pc from the star where the extremely diffuse wind bubble begins. At the edge of the bubble is a shell of density $\approx 1\mathrm{cm}^{-3}$. The clumps are assumed to exist everywhere outside of the initial piston and have a temperature of 2×10^4 K. The bubble, CSM and clumps are all in pressure balance with the external ISM.

The bubble, CSM material and the clump gas are assumed to be in collisional ionization equilibrium at their appropriate temperatures until they are engulfed by the remnant, from which point the non-equilibrium ionization is calculated along with the hydrodynamics.

In all, 6 different models are considered, whose parameters are listed in Table 1. The chief parameter is the maximum mass loading rate Q, for which we consider values between 0 and 2.1×10^{-36} g cm^{-3} s^{-1}. We parameterize the mass loading rate by X, which is measured in units of the characteristic mass loading rate, $Q_c = 2.1 \times 10^{-39}$ g cm^{-3} s^{-1}. In all models, the density in the wind bubble is set to 10^{-3} cm^{-3}. In Table 1, L refers to LMC H II region abundances and G signifies galactic SNR abundances.

TABLE 1

MODEL PARAMETERS AND MAXIMUM X-RAY FLUX IN THE EINSTEIN SOFT BAND

	Parameters			Properties at Maximum Brightness			
Model	n_{bub} (cm^{-3})	X (Q_c)	Abundance	Radius (pc)	Age (yr)	L_X (erg s^{-1})	Hardness Ratio
1	0.001	0	L	51.2	34900	2.0×10^{34}	0.26
2	0.001	10	L	57.9	131900	4.9×10^{34}	0.04
3	0.001	30	L	52.7	69600	1.0×10^{35}	0.04
4	0.001	100	L	52.3	96900	5.1×10^{35}	−0.22
5	0.001	100	G	52.2	94700	6.5×10^{35}	−0.26
6	0.001	1000	L	34.1	47500	1.6×10^{36}	−0.15

5.2. Hydrodynamic Evolution of the Models

Figure 1 (*Left*) shows the density, velocity, temperature and Mach number for model 1 (no mass loading) at a time when the reflected shock has traversed back through the outer fifth of the remnant and heated the gas to more than 10^7 K. The density in the bubble remains very low. At the same time, a transmitted shock is being driven into the bubble wall, producing a thin, dense, radiative shell, which has a velocity of ~ 100 km s^{-1} .

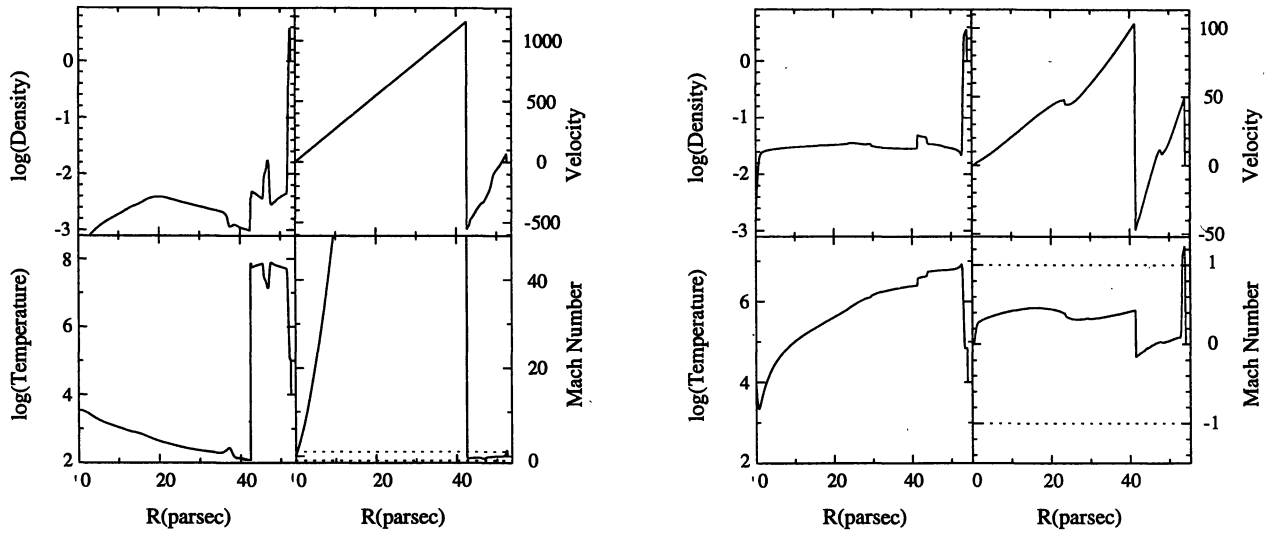

Fig. 1. *Left*: Hydrodynamic variables of model 1 as a function of radius (pc), at the time of maximum X-ray brightness listed in Table 1. Top left panel shows total ion number density (cm^{-3}); top right panel shows gas velocity (km s^{-1}); bottom left panel shows gas kinetic temperature (K); bottom right panel shows the flow Mach number. Dotted lines indicate Mach numbers of ± 1. *Right*: Same as *Left* but for model 3.

Model 3, with a mass loading parameter $X = 30$, also hits the bubble wall to produce a transmitted and reflected shock. This model is shown at an age of 69 600 years in Figure 1 (*Right*). The reflected shock has got back to a radius of $\sim$ 40 pc, but it can be seen that the shock is substantially weaker than in model 1. In addition, the mass loading has raised the density and temperature throughout the bubble, including the parts that have not yet been reached by the reverse shock. When the mass loading parameter is increased to $X = 100$, as in model 4, then the mass loading dominates the dynamics of the remnant. Figure 2 (*Left*) shows this model at an age of 96 900 years, 40 000 years after the remnant has hit the edge of the bubble. A reflected/transmitted shock pair is again produced by the interaction between the remnant and the bubble wall but this time the weakness of the reflected shock (Mach number approximately 1.3) means that it propagates

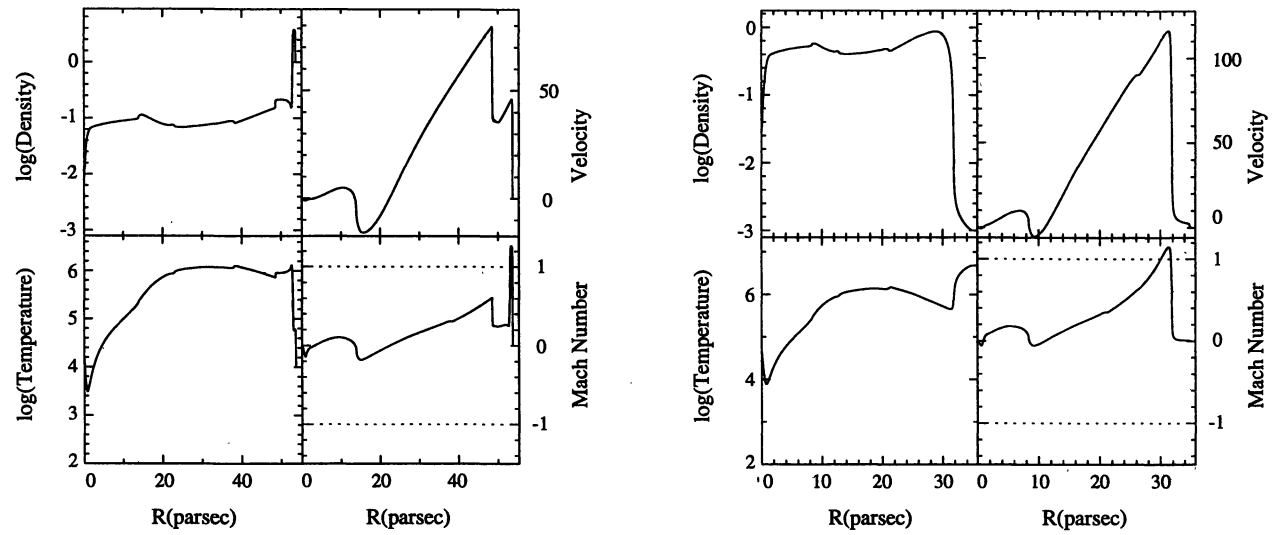

Fig. 2. *Left*: Same as Fig. 1 (*Left*), but for model 4. *Right*: Same as Fig. 1 (*Left*), but for model 6.

very slowly back into the bubble and fails to reverse the sign of the velocity of the remnant gas. The gas with negative velocities in the center of the remnant is due to the high pressure that builds up in the mass loading regions. A pressure gradient develops that decelerates the inner parts of the remnant and eventually causes them to flow back towards the center. The density in the interior of the bubble is now quite high (0.1 cm^{-3}) and the temperature reaches 10^6 K because of drag heating from the mass loading process. Due to conservation of momentum, the remnant decelerates as more and more mass is added and this "drag" due to the clump mass causes the temperature inside the remnant to rise. In reality, enhanced cooling in the turbulent mixing regions where the clump mass finally enters the ablating flow may reduce this viscous heating but by a degree that is hard to estimate quantitatively.

Increasing the mass loading parameter still further to $X = 1000$, as in model 6, causes the remnant to stall before reaching the bubble wall. Figure 2 (*Right*) shows the remnant before this has happened, at an age of 47 500 years. As in the previous case, a high pressure builds up in the mass loading regions and decelerates the inner parts of the remnant. In this case, the mass loading rate is so high that the pressure becomes great enough to reverse the direction of flow of this gas so that it flows back towards the center supersonically. The density in the remnant is now nearly 1 cm^{-3} throughout the volume, and the gas cools rapidly after this point.

Using galactic instead of LMC abundances (model 5) enhances the cooling somewhat, but this has almost no impact on the dynamics.

5.3. X-ray Emission of Models

Figure 3 shows the evolution of the X-ray luminosity with time in the Einstein band (0.16 to 3.5 keV) for some of the models described in Table 1, together with the corresponding evolution of the hardness ratio, defined by the ratio of the difference of the luminosities in the bands $0.16-0.6$ keV and $0.8-3.5$ keV to the sum of these luminosities. The X-ray luminosity plotted is that intrinsic to the source, whereas we have assumed an absorbing column density of 3×10^{21} $m_{\rm H}$ cm^{-2}, in agreement with other authors (e.g., WH91), when calculating the hardness ratios.

Only the models with moderate to high mass loading rates are shown as these are the only ones that give sufficient X-ray luminosity. It can be seen that higher mass loading rates lead to higher and earlier peak luminosities, but to more rapid fading. Increasing the metal abundance while maintaining the same mass loading rate leads to a slight increase in the X-ray luminosity. In each case the peak luminosity coincides with the minimum hardness ratio. The effect of different abundances is more marked in the hardness ratio. The model with the higher metal abundance is consistently softer than the equivalent model with LMC abundances.

6. DISCUSSION

Any model that seeks to explain the diffuse X-ray emission from OB associations in the LMC should fulfill the following criteria (WH91): (i) produce an X-ray luminosity in the Einstein band of $0.2-6\times10^{35}$ erg s^{-1} with hardness ratios between -0.11 and 0.4 (ii) produce surface brightness profiles consistent with observed

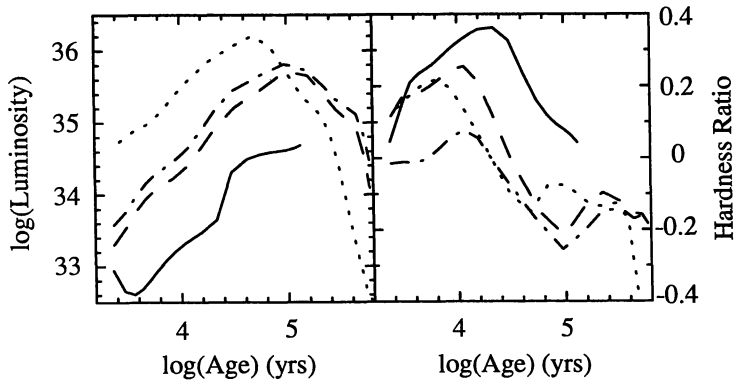

Fig. 3. Evolution with time of intrinsic X-ray luminosity (erg s^{-1}) and Einstein hardness ratio of models 3 (solid line), 4 (dashed line), 5 (dot-dashed line), and 6 (dotted line).

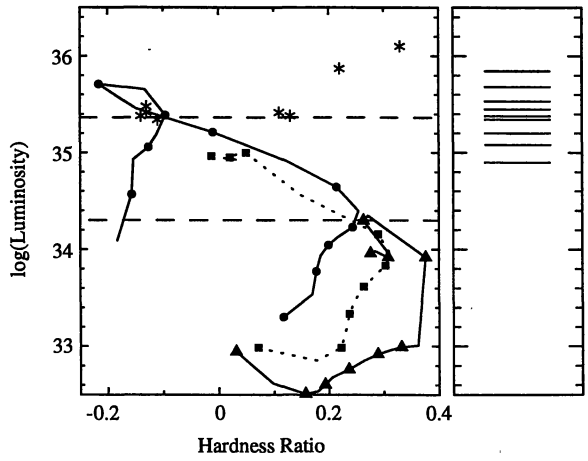

Fig. 4. Color-luminosity diagram showing measured values of luminosity (erg s^{-1}) and hardness ratio from WH91 (star symbols), together with evolutionary tracks for model 1 (triangles), model 3 (squares), and model 4 (circles). Measured luminosities for which no corresponding hardness ratios are available (WH91) are shown in the right hand panel by horizontal lines.

morphologies (iii) produce velocities of $30-40$ km s^{-1} for the Hα filaments (iv) produce X-ray emitting lifetimes consistent with star formation and supernova rates in the LMC ($\sim 10^5$ yr). We discuss each of these requirements in the following discussion.

From Figure 3 we see that our models 3, 4, 5 and 6 produce X-ray luminosities and hardness ratios in the correct range. In Figure 4, X-ray luminosity is plotted against hardness ratio for models 1, 3 and 4. In this figure, the observations from WH91 are also shown (star symbols and horizontal bars). It can be seen that models 3 and 4 (with mass loading factors of $X = 30$ and $X = 100$, respectively) agree with most of the observations, while model 1 ($X = 0$, no mass loading) does not agree at all.

It is found that the mass loaded models can reproduce any X-ray morphology. For the case $X = 30$, the X-ray emission is highest behind the reflected shock and the peak emission follows the shock in towards the center of the remnant. This results in a broad shell morphology. In the $X = 100$ case, the mass loading raises the temperature and density throughout the remnant to almost constant distributions, resulting in a virtually flat X-ray surface brightness profile.

If we assume that it is cooling behind the radiative transmitted shock that is responsible for the Hα filaments, then only models with mass loading factors $X \geq 30$ lead to Hα shell velocities of $40 - 50$ km s^{-1}, consistent with those observed (Meaburn & Terrett 1980; Meaburn & Blades 1980). Lower mass loading factors result in faster transmitted shocks. However, we note that it is possible for a cluster of some few tens of O stars, each with a stellar wind terminal velocity $V_* \simeq 2000$ km s^{-1} and mass loading rate of 10^{-6} $M_\odot$ yr^{-1} to account for the kinematics of the Hα filaments (Arthur & Henney 1995).

WH91 estimate that the mean X-ray observable lifetime of supernova-heated bubbles must be $\sim 10^5$ years if they are to explain the observed X-ray emission. As can be seen from Figure 3, the X-ray emitting lifetime of our models is quite a strong function of mass loading rate. All models with $X > 10$ have a sufficiently long X-ray observable lifetime. For moderate mass loading rates the lifetime increases with X, but for $X > 100$, cooling is strongly enhanced and the lifetime falls off.

7. CONCLUSIONS

The discussion above shows that the mass loaded supernova remnant model can explain in a natural fashion many of the puzzling X-ray properties of OB associations in the Large Magellanic Cloud. Models with mass loading rates between 6.3×10^{-38} and 6.3×10^{-37} g cm^{-3} s^{-1} ($X = 30$ and $X = 300$) are consistent in a general way with the statistics of the excess X-ray emission coincident with LMC OB associations. The mass loading rates demanded of the models are quite plausible, falling several orders of magnitude below the canonical value derived in Arthur & Henney (1995). Analysis of results from the ROSAT survey of the LMC, when complete, should provide much more stringent constraints on the models.

The numerical calculations in this paper were carried out on the UNAM Cray YMP4/464 administered by DGSCA. We would like to thank H. Lloyd for providing the original version of the Raymond-Smith code, A. Raga for some timely comments and A. Santillán for liaising with DGSCA. Part of this work was carried out while the authors were in receipt of Cátedras Patrimoniales de Excelencia from CONACyT, México.

REFERENCES

Anders, E., & Grevesse, N. 1989, Geochim. Cosmochim. Acta, 53, 197
Arthur, S. J. 1991, Ph.D. thesis, University of Leeds
Arthur, S. J., Dyson, J. E., & Hartquist, T. W. 1993, MNRAS, 261, 425 (ADH1)
————. 1994, MNRAS, 269, 1117 (ADH2)
Arthur, S. J., & Falle, S. A. E. G. 1991, MNRAS, 251, 93
————. 1993, MNRAS, 261, 681
Arthur, S. J., & Henney, W. J. 1995, ApJ, accepted
Chu, Y.-H., & Mac Low, M.-M. 1990, ApJ, 365, 510 (CML90)
Dufour, R. J. 1984, in Structure and Evolution of the Magellanic Clouds, ed. S. van den Berg & K. S. de Boer, (Dordrecht: Reidel), 353
Dyson, J. E., & Hartquist, T. W. 1992, Astro. Lett. and Comm., 28, 301
Falle, S. A. E. G. 1991, MNRAS, 250, 581
García-Segura, G., & Mac Low, M. M. 1995, ApJ, accepted
Godunov, S. K. 1959, Mat. Sb., 47, 271
Gull, S. 1973, MNRAS, 161, 47
Hamilton, A. J. S., Sarazin, C. L., & Chevalier, R. A. 1983, ApJS, 51, 115
Hartquist, T. W., Dyson, J. E., Pettini, M., & Smith, L. J. 1986, MNRAS, 221, 715 (HDPS)
Hartquist, T. W., & Dyson, J. E. 1993, QJRAS, 34, 57
Mac Low, M.-M., McKee, C. F., Klein, R. I., Stone, J. M., & Norman, M. L. 1994, ApJ, 433, 757
Meaburn, J., & Blades, J. C. 1980, MNRAS, 190, 403
Meaburn, J., & Terrett, D. C. 1980, A&A, 89, 126
Pagel, B. E. J. 1993, in New Aspects of Magellanic Cloud Research, ed. B. Baschek, G. Klare, & J. Lequeux, (Berlin: Springer Verlag), 330
Raymond, J. C., & Smith, B. W. 1976, ApJS, 35, 419
Russell, S. C., & Dopita, M. A. 1990, ApJS, 74, 93
————. 1992, ApJ, 384, 508
Vishniac, E. T. 1983, ApJ, 274, 152
Wang, Q., & Helfand, D. J. 1991, ApJ, 373, 497 (WH91)